Japanese Journal of Applied Physics
Vol. 45, No. 3B, 2006, pp. 1904–1908

Feed-Forward Compensation for High-Speed Atomic Force Microscopy Imaging of Biomolecules

Takayuki UCHIHASHI[1,2*], Noriyuki KODERA[1], Hisanori ITOH[1], Hayato YAMASHITA[1] and Toshio ANDO[1,2,3]

[1]*Graduate School of Natural Science and Technology, Kanazawa University, Kakuma-machi, Kanazawa 920-1192, Japan*
[2]*CREST, Japan Science and Technology Agency (JST), 4-1-8 Honcho, Kawaguchi, Saitama 332-0012, Japan*
[3]*Frontier Science Research Organization, Kanazawa University, Kakuma-machi, Kanazawa 920-1192, Japan*

(Received July 3, 2005; accepted November 28, 2005; published online March 27, 2006)

High-speed imaging by atomic force microscopy (AFM) requires the implementation of a fast control of tip–surface distance to maintain a constant interaction force. In particular, a well-controlled low load force is essential for observing soft biological molecules without causing damage to the sample. The accurate control of tip–surface distance where only feedback control is used is intrinsically difficult particularly for fast scanning. Here, we demonstrate that the combination of feedback and feed-forward control is useful for a more accurate distance control. We evaluate the bandwidth performance of the closed loop with and without feed-forward compensation using a model AFM system.We show that the combination of feedback and feed-forward control yields a greater than two fold improvement in bandwidth. We have applied this technique to the observation of myosin V and actin filaments at a high scanning rate. [DOI: 10.1143/JJAP.45.1904]

KEYWORDS: atomic force microscope, high-speed imaging, protein, feed-forward compensation

1. Introduction

Biomolecules such as protein and nucleic acid function via intermolecular interaction and structural changes. Therefore, to elucidate the molecular function and expression mechanisms, it is highly desirable to observe the dynamic processes of individual molecules. To date, there has been no measurement technique with both sufficient spatial and temporal resolutions.

Atomic force microscopy (AFM) is well known as a powerful tool for observing individual molecular structures with a high resolution in an aqueous solution.[1)] However, conventional AFM does not have a sufficient time resolution. Typically a few minutes are required to take one image. This slow scan speed is ineffective for samples that move quickly and undergo rapid structural changes. Although several attempts to improve the scan performance of AFM have been carried out to date, the image capture rate has remained at several frames per second or less.[2–5)] Recently, Humphris *et al.* achieved an imaging rate of less than 20 ms/frame using a microresonator as a sample stage.[6)] However, as this technique is based on the contact mode without feedback control, it can be used only for samples that are hard, robust and tightly fixed onto a substrate. In 2001, we developed a high-speed AFM that can image soft biomolecules at 80 ms/frame in the tapping mode.[7,8)]

In order to achieve high-speed AFM imaging, all the devices that compose the AFM system must exhibit a fast response. The development of various devices, such as small cantilevers,[9)] and high-speed deflection sensors, and techniques, such as amplitude detection,[8)] active damping of the scanner[10)] and dynamic proportional, integral and derivative (PID) feedback control,[11)] have made high-speed measurement feasible. However, to carry out measurements on soft biological samples, it is necessary to decrease loading force from the tip. In tapping-mode AFM, the averaged loading force F_a at a cantilever resonant frequency is given by:

$$F_a = k \times (A_0 - A_s)/Q, \tag{1}$$

where k is the spring constant of the cantilever, A_0 is the free oscillation amplitude of the tip, A_s is the set-point amplitude for the feedback control and Q is the quality factor of the cantilever. In order to reduce loading force, it is necessary to bring set-point amplitude close to free oscillation amplitude. However, feedback bandwidth decreases as set-point amplitude approaches free amplitude.

Now, suppose the cantilever is scanning over the steepest down hill of a sample having a sinusoidal wave shape with a height of h and a periodicity of λ, and the sample stage is moved horizontally at a velocity of V_s. The spatial frequency of $1/\lambda$ is converted to a temporal frequency of $f \equiv V_s/\lambda$, which corresponds to the required feedback bandwidth. After one cycle of the cantilever's oscillation at a frequency of f_c, sample height is lowered by $h\sin(\Delta\theta/2)$, where $\Delta\theta = (f/f_c) \times 2\pi$. If, however, the sample surface is not present, the cantilever's tip end would go by $A_0 - A_s$ at the downswing. The oscillation tip should touch the sample surface at the bottom of every swing. Hence, the following relationship should hold.

$$f < \frac{f_c}{\pi} \sin^{-1}\left(\frac{A_0 - A_s}{h}\right) \tag{2}$$

From this relationship, in order to increase feedback bandwidth, $A_0 - A_s$ should be increased. Thus, the two aspects of soft tapping and fast imaging are in conflict.

In this study, we employed feed-forward compensation in conjunction with feedback control to satisfy these two conflicting requirements. This technique was already implemented in contact-mode AFM by Schitter *et al.*[12)] However, the quantitative evaluation of its performance and the high-speed AFM imaging of soft biomolecules have not yet been carried out. An evaluation of bandwidth with and without feed-forward compensation shows that we can effectively increase feedback bandwidth. Furthermore, we have applied this technique to the fast imaging of soft biomolecules.

2. Experimental

We used a laboratory-built high-speed AFM, the details of which are described in previous papers.[7,8)] AFM images were acquired in the tapping mode. The cantilever we used

*E-mail address: tuchi@kenroku.kanazawa-u.ac.jp

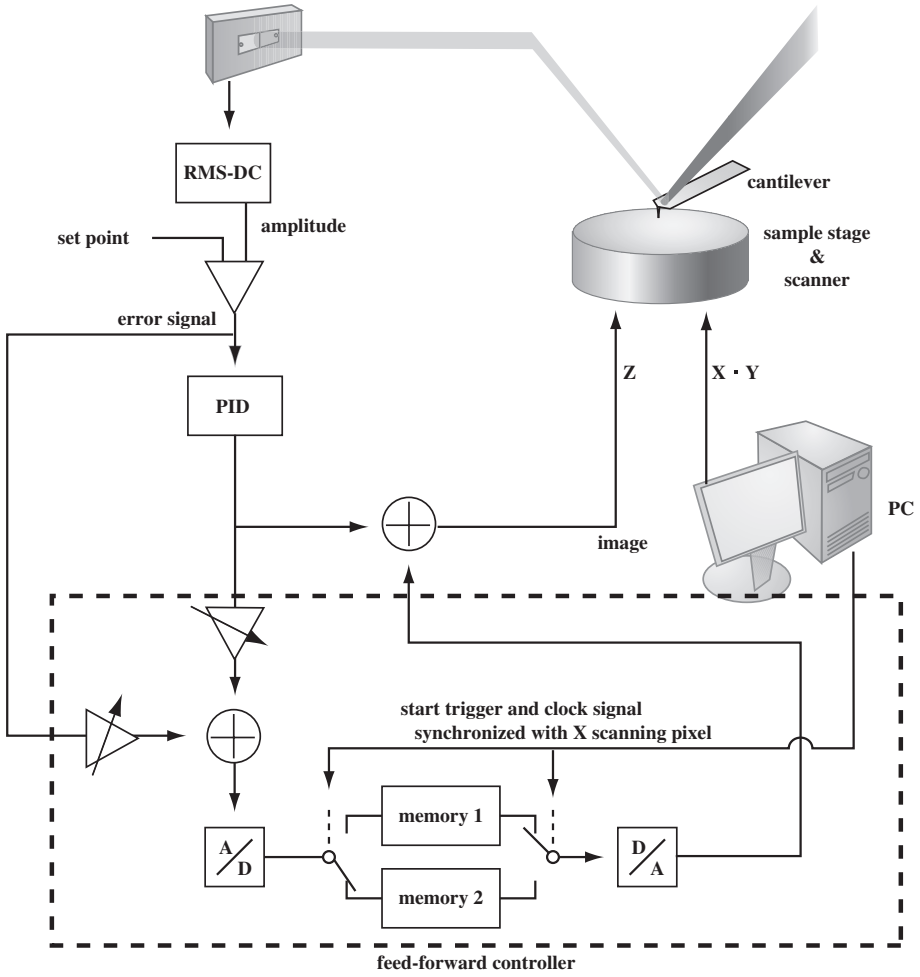

Fig. 1. Block diagram of combination control of feedback and feed-forward.

was a specially designed one provided by Olympus; its resonant frequency was about 800 kHz in water and the spring constant was about 100 pN/nm. The carbon tip was grown on the cantilever by electron beam deposition.

Figure 1 shows a block diagram of the combination of the feedback and feed-forward control. The feed-forward controller consists of 12 bit D/A, A/D converters, two memories and two high-speed analogue switches. The feed-forward controller starts to record the input signal to memory 1 triggered by the start signal from the scan controller. The input signal is recorded into memory 1 synchronized with the clock signal of scanning pixel. After the clock number reaches the predetermined number, which is the same as the pixel number of the X scanning line, the recorded signal is output from memory 1 synchronized with the clock, and simultaneously the input signal is recorded in memory 2. These processes are repeated until one frame is completed. The addition signal of the PID feedback and error signals are used as the input signal for the first X scanning line. After the second X line, the addition signal of the PID, error and also feed-forward signals are recorded. It should be noted that the error signal is also used as the feed-forward signal. In an aqueous environment, the Q value of the cantilever is not so large, typically less than 5. Therefore, the error signal reflects the deviation of the tip trajectory from the actual geometry, which is essential for compensating the feedback delay. The input gain of the feed-forward signal for the PID output is set at lower than 1, typically 0.5, because, when the surface geometry would rapidly change in each line, a large feed-forward gain increases the inaccuracy of the topographic measurement on the contrary. On the other hand, the gain of the error signal is set at about 0.1, which is basically decided by the ratio of the inversed optical lever sensitivity of the deflection sensor and the piezoelectric constant. In our case, they are about 15 and 90 nm/V, respectively. Therefore, the gain of the error signal should be less than 0.17.

To facilitate the quantitative performance evaluation of feed-forward compensation, we used a mock AFM circuit consisting of a second-order low-pass filter with the same resonance properties of the Z-scanner, and a threshold circuit that can simulate a decrease in the cantilever's oscillation caused by the tip–sample contact. A mock sample topography was produced by a function generator. The details of this circuit will be given in a separate paper. For the evaluation using the mock AFM circuit, the oscillation frequency and amplitude of the mock cantilever were set at 800 kHz and 0.1 V, respectively. A sinusoidal wave with a frequency of 7.3 kHz and an amplitude of 0.1 V was used as the mock sample topography.

3. Results and Discussion

Figure 2 shows a comparison of pseudo-AFM images produced by the mock AFM circuit without and with feed-

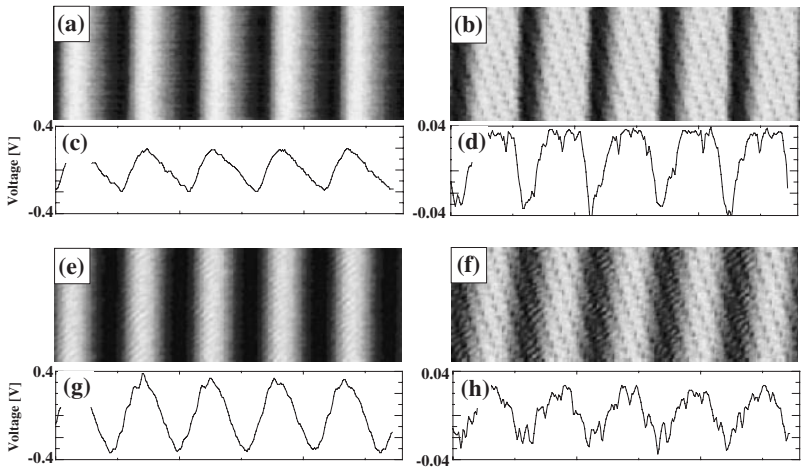

Fig. 2. Pseudo-AFM images produced by mock AFM under only feedback [(a)–(d)] and combination control [(e)–(h)]. Topography [(a) and (e)], topographic cross-sectional profiles [(c) and (g)], error images [(b) and (f)] and error cross-sectional profiles [(d) and (h)]. The feed-forward gain and error gain are 0.5 and 0.1, respectively.

forward compensation. Here, the set-point amplitude for feedback control was set at 98% of the cantilever's free amplitude. The scan direction was from left to right. As shown in Figs. 2(a) and 2(c), the topography in the case of without feed-forward compensation exhibits a distorted sinusoidal shape because the tip cannot touch the surface, as the surface topography has lowered due to the large set-point amplitude. On the other hand, as shown in Figs. 2(e) and 2(g), using feed-forward compensation the topography shows a sinusoidal shape. The height difference in the case of with the feed-forward compensation increases about 180% compared with that without feed-forward compensation. Also, the error signal in the case of with feed-forward compensation decreases to about 85% of that without feed-forward compensation as shown in Figs. 2(d) and 2(f).

To quantitatively evaluate the bandwidth in the case of the combination of feedback and feed-forward controls, we measured the phase difference between the sinusoidal wave of the mock sample topography and the signal applied to the mock *Z*-scanner. Figure 3 shows the phase delay in the case of the combination controller with respect to the mock sample topography as a function of the frequency of the mock sample topography for different set-point values. The closed circles and triangles correspond to phase delay measured with only the feedback control at the set-point amplitudes of 98 and 80%, respectively. The open circles and triangles correspond to the phase delay under the combination control with feed-forward compensation at the set-point amplitudes of 98 and 80%, respectively. In the case of 98% set-point amplitude, the phase delay in the case of without feed-forward compensation is significant and the bandwidth, which is defined as the frequency at which the phase of 45 deg is delayed, is about 9 kHz. However, with the addition of feed-forward compensation, the bandwidth is improved to 51 kHz. In the case of 80% set-point amplitude, the bandwidths for without and with feed-forward compensations are about 31 and 70 kHz, respectively. Thus, bandwidth is significantly improved by the combination of the feedback and feed-forward controls. This evaluation was carried out under the ideal condition that the topography did not change each *X* scanning line. However, as long as the topographies of individual *X* lines are not markedly different, feed-forward compensation works even though the extension of bandwidth is suppressed.

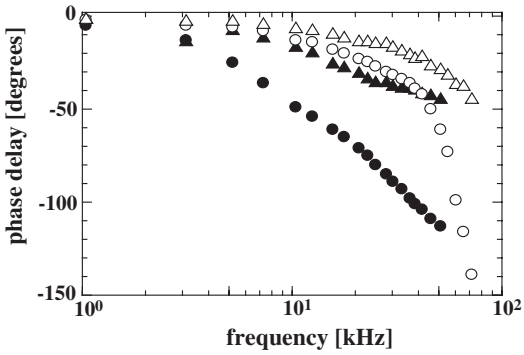

Fig. 3. Phase delay in the case of feedback and combination control with recpect to the mock sample topography as function of frequency of mock sample topography. The closed circles and triangles correspond to phase delay measured with only the feedback control at the set-point amplitudes of 98 and 80%, respectively. The open circles and triangles correspond to phase delay under the combination control at the set-point amplitudes of 98 and 80%, respectively.

To confirm the validity of this technique, we measured soft biomolecules at a high speed. Figures 4(a) and 4(b) show high-speed AFM images of myosin V taken at 60 ms/frame without and with feed-forward compensation, respectively. The scan size was $150 \times 150\,\mathrm{nm}^2$. The scan direction was from right to left on the images. In comparison with the topographic images, we can note that the contour of the myosin molecule where the feed-forward compensation is employed becomes clearer than that taken with only the feedback control. Figures 4(c) and 4(d) show the cross sections of topographic and error images at the line indicated by white broken lines in Figs. 4(a) and 4(b), where this part of the molecule does not move very much in each frame. The solid and dotted lines correspond to the cross sections of the images with and without feed-forward compensation, respectively. We can observe that the height difference is slightly increased by using feed-forward compensation. Also, in the feed-forward controlled system, it can be noted

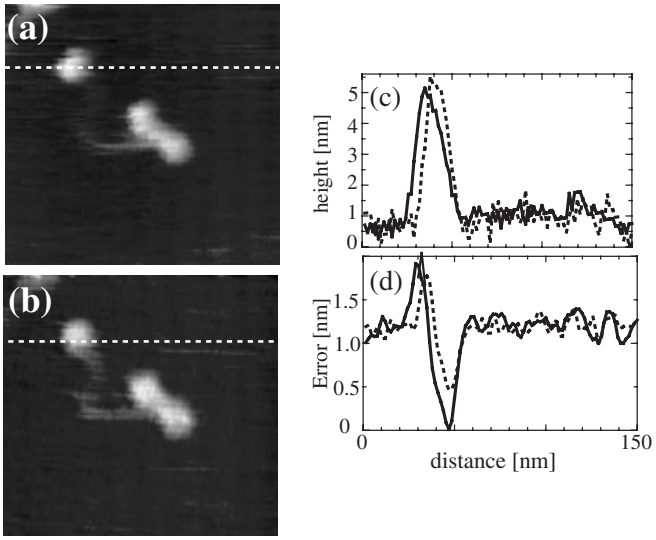

Fig. 4. High-speed AFM images of myosin V taken at 60 ms/frame with (a) feedback and (b) combination control, respectively. The scan size was $150 \times 150\,nm^2$ with 200×200 pixels. The cross-sectional profiles for the (c) topographic and (d) error images measured with feedback (solid lines) and combination control (broken lines) are compared. The cross-sectioned part of the image is indicated by white broken lines on the images. The images were scanned from right to left scan.

that the rising edge of the topography becomes steep, which means that the phase delay is compensated. On the other hand, the error signal decreases to 60% with the addition of feed-forward compensation.

Figure 5 shows successive images of myosin V captured at 37 ms/frame with a scan size of $100 \times 100\,nm^2$. These images were taken under a combination of feedback and feed-forward control. Although it is difficult to observe from these six images, some parts of the molecule, particularly those surrounded by a white broken circle, are moving in every frame probably due to Brownian motion. Thus, the combination of feedback and feed-forward control works even for moving samples.

Actin is a more fragile protein than myosin V. Therefore it is more difficult to clearly observe it at high speeds without damaging the sample. Figures 6(a) and 6(b) shows topographic images taken with and without feed-forward compensation, respectively. These images were acquired at 60 ms/frame. The set-point amplitude for feedback control was 90% of the free amplitude of 2.5 nm. In Fig. 6(a), we can observe the half pitches of the double-helix turn of a filament. After feed-forward compensation is cut, the right side of the filament trails and the image quality deteriorates markedly. In order to improve image quality, the set-point amplitude should be decreased to about 80% of the free

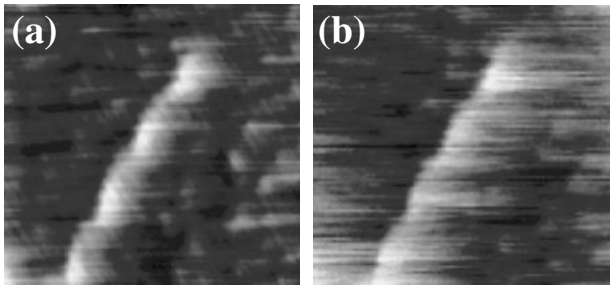

Fig. 6. AFM images of actin filament measured under (a) feedback and (b) combination control. These images were acquired at 60 ms/frame. The set-point amplitude for feedback control was 90% of the free amplitude of 2.5 nm. The scan size was $200 \times 200\,nm^2$ with 100×100 pixels.

amplitude. In that case, however, the actin filament is easily swept out by the AFM tip. Since the quality factor and the spring contant of the cantilever used here were about 3 and 100 pN/nm, respectively, the loading forces with and without feed-forward compensation were about 8 and 17 pN, respectively. Therefore, in this case, the loading force could be reduced to about one-half by feed-forward compensation.

Figure 7 shows successive images of an actin filament taken at 60 ms/frame. The set-point amplitude was 91% of the free oscillation amplitude of 18 nm, which is a relatively large amplitude. The image shown in Fig. 7(a) was taken under the combination control. Although this image was captured after 59 frames from the first scan, the actin filament suffered only minor damage. Figures 7(b)–7(f) show the images taken with only feedback control imediately after the image shown in Fig. 7(a) was captured. They are displayed every eight frames. In the case of feedback control alone, not only does the image quality deteriorate, the actin filament is also easily destroyed. From these results, we can note that feed-forward compensation is useful for the clear imaging of fragile molecules at a small loading force.

4. Conclusions

In summary, we have applied feed-forward compensation to high-speed AFM for observing biological molecules. By feed-forward compensation in conjunction with feedback control, the tip can trace a surface more accurately, which increases measured height and decreases error signal. Bandwidth evaluation using the mock AFM circuit showed that the bandwidth in the case of combination control is more than twice that with only feedback control. When applied to the fast imaging of myosin V and actin filaments, this new technique improves image quality and decreases

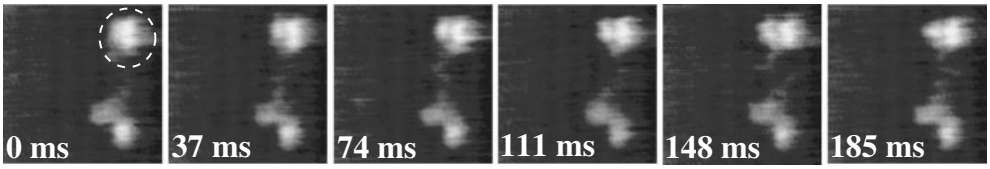

Fig. 5. Successive AFM images of myosin V captured at 37 ms/frame under combination control. The scan size is $100 \times 100\,nm^2$ with 100×100 pixels.

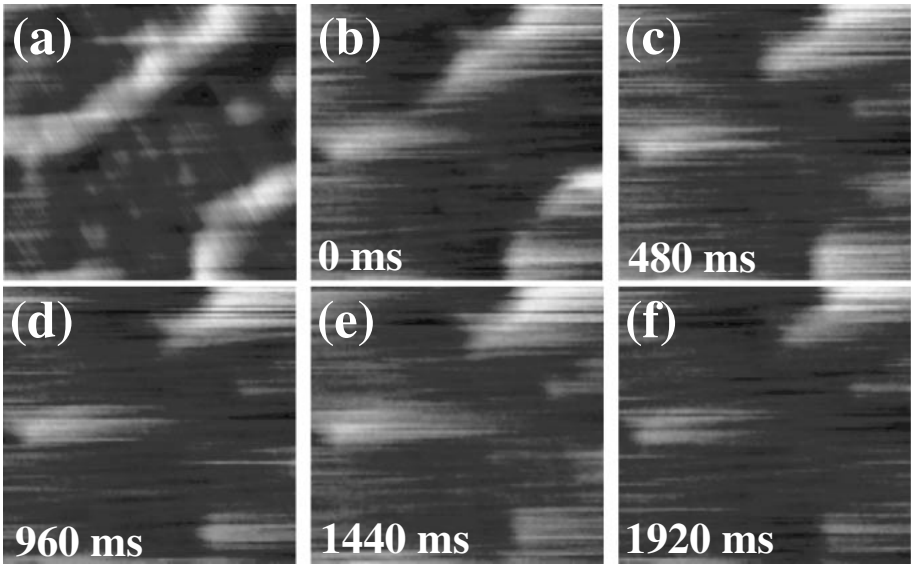

Fig. 7. Successive images of actin filament taken at 60 ms/frame under (a) the combination and (b)–(f) the feedback control. The set-point amplitude was 91% of the free oscillation amplitude of 18 nm. For (b)–(f), images are displayed every eight frames. The scan size was $200 \times 200\,\mathrm{nm}^2$ with 100×100 pixels.

phase delay even at a scanning rate of 60 ms/frame. Also the destruction of fragile actin filaments is minimized. Thus, this technique can compensate the insufficient bandwith of feedback control and offers a significant improvement for the soft imaging of fragile biomolecules with fast scanning.

Acknowledgements

This research was supported by Core Research for Evolutional Science and Technology (CREST) of the Japan Science and Technology Agency (JST) and Industrial Technology Research Grant Program in '04 from New Energy and Industrial Technology Development Organization (NEDO).

1) H. G. Hansma, J. Vesenka, C. Siegerist, G. Kelderman, H. Morrett, R. L. Sinsheimer, V. Elings, C. Bustamante and P. K. Hansma: Science **256** (1992) 1180.
2) M. B. Viani, T. E. Schæffer, G. T. Paloczi, L. I. Pietrasanta, B. L. Smith, J. B. Thompson, M. Richter, M. Rief, H. E. Gaub, K. W. Plaxco, A. N. Cleland, H. G. Hansma and P. K. Hansma: Rev. Sci. Instrum. **70** (1999) 4300.
3) T. Sulchek, R. Hsieh, J. D. Adams, S. C. Minne, C. F. Quate and D. M. Adderton: Rev. Sci. Instrum. **71** (2000) 2097.
4) T. Sulchek, G. G. Yaralioglu, C. F. Quate and S. C. Minne: Rev. Sci. Instrum. **73** (2002) 2928.
5) B. Rogers, T. Sulchek, K. Murray, D. York, M. Jones, L. Manning, S. Malekos, B. Beneschott, J. D. Adams, H. Cavazos and S. C. Minne: Rev. Sci. Instrum. **74** (2003) 4683.
6) A. D. L. Humphris, M. J. Miles and J. K. Hobbs: Appl. Phys. Lett. **86** (2005) 034106.
7) T. Ando, N. Kodera, D. Maruyama, E. Takai, K. Saito and A. Toda: Proc. Natl. Acad. Sci. U.S.A. **98** (2001) 12468.
8) T. Ando, N. Kodera, D. Maruyama, E. Takai, K. Saito and A. Toda: Jpn. J. Appl. Phys. **41** (2002) 4851.
9) M. Kitazawa, K. Shiotani and A. Toda: Jpn. J. Appl. Phys. **42** (2003) 4844.
10) N. Kodera, H. Yamashita and T. Ando: Rev. Sci. Instrum. **76** (2005) 053708.
11) T. Ando, T. Uchihashi, N. Kodera, A. Miyagi, R. Nakakita and H. Yamashita: to be submitted to the STM05 conference paper.
12) G. Schitter, F. Allgœwer and A. Stemmer: Nanotechnology **15** (2004) 108.